GDCh

Research Articles

Angewandte
Chemie
International Edition
www.angewandte.org

Gas Separation

A Microporous Metal-Organic Framework with Unique Aromatic Pore Surfaces for High Performance C_2H_6/C_2H_4 Separation

Yingxiang Ye, Yi Xie, Yanshu Shi, Lingshan Gong, Joshua Phipps, Abdullah M. Al-Enizi, Ayman Nafady, Banglin Chen,* and Shengqian Ma*

Abstract: Developing adsorptive separation processes based on C_2H_6-selective sorbents to replace energy-intensive cryogenic distillation is a promising alternative for C_2H_4 purification from C_2H_4/C_2H_6 mixtures, which however remains challenging. During our studies on two isostructural metal–organic frameworks (**Ni-MOF 1** and **Ni-MOF 2**), we found that **Ni-MOF 2** exhibited significantly higher performance for C_2H_6/C_2H_4 separation than **Ni-MOF-1**, as clearly established by gas sorption isotherms and breakthrough experiments. Density-Functional Theory (DFT) studies showed that the unblocked unique aromatic pore surfaces within **Ni-MOF 2** induce more and stronger C–H⋯π with C_2H_6 over C_2H_4 while the suitable pore spaces enforce its high C_2H_6 uptake capacity, featuring **Ni-MOF 2** as one of the best porous materials for this very important gas separation. It generates $12 \, L \, kg^{-1}$ of polymer-grade C_2H_4 product from equimolar C_2H_6/C_2H_4 mixtures at ambient conditions.

Introduction

Ethylene (C_2H_4) is one of the most widely used petrochemical feedstocks, with a global production capacity reaching over 210 million tons in 2021. Currently, C_2H_4 is derived primarily from steam cracking of naphtha and ethane (C_2H_6) before further purification by repeated cryogenic distillation cycling under harsh conditions.[1] Because of their highly similar molecular size and volatility, C_2H_4/C_2H_6 separation is difficult and is one of the most energy-intensive processes consuming up to $\approx 800 \, PJ$ of energy per year.[2] Replacing

traditional distillation to purify ethylene through adsorptive separation process based on porous materials would lead to tremendous global benefits. Generally, the separation of C_2H_4/C_2H_6 mixtures can be implemented by C_2H_4-selective or C_2H_6-selective sorbents.[3] In comparation with the well-explored C_2H_4-selective sorbents,[4] using C_2H_6-selective adsorbents provides a more energy efficient strategy as it can produce high purity C_2H_4 through a single separation process.[5]

Metal-organic frameworks (MOFs), an emerging class of customizable porous materials, have been extensively explored as adsorbents for gas separation/purification due to their highly structural modularity and abundant functionality.[6] To realize the C_2H_6-selective MOFs, it needs to minimize the framework's interactions with C_2H_4 while maximize its interactions with C_2H_6, which is very difficult and challenging, because typical functional sites, particularly open metal sites, have stronger interactions with C_2H_4 than C_2H_6.[7] To make use of the slightly higher polarizability of C_2H_6 over C_2H_4 (44.7×10^{-25} vs $42.52 \times 10^{-25} \, cm^3$),[8] a few microporous MOFs with nonpolar/inert pore surfaces has been discovered for C_2H_6/C_2H_4 separation.[9] Among reported microporous MOFs for C_2H_6/C_2H_4 separation, [Cu-(Qc)$_2$] with aromatic quinoline pore surfaces induce the stronger interactions with C_2H_6 over C_2H_4 through multiple C–H⋯π interactions, providing the promising strategy of developing C_2H_6 adsorptive MOF materials though not well developed yet.[9d] In this report, we used two organic linkers with rich aromatic moieties, btz (btz=1,4'-bis(4H-1,2,4-triazol-4-yl)benzene) and bdp (H_2bdp=1,4-benzenedipyrazole), respectively, to construct two isostructural Ni-based MOF materials, [Ni(btz)Cl]·Cl (**Ni-MOF 1**), and [Ni(bdp)] (**Ni-MOF 2**). The Cl^- ions inside the pores of **Ni-MOF 1** not only block part of the pore spaces, but also significantly affect the effective roles of the three aromatic rings for their C–H⋯π interactions with C_2H_6 molecules, so this MOF does not show any C_2H_6/C_2H_4 separation performance. Whereas the naked pore spaces within **Ni-MOF 2** enable full utilization of the three aromatic rings of the bdp organic linkers for their multiple and stronger C–H⋯π interactions with C_2H_6 molecules over C_2H_4 ones thereby affording **Ni-MOF-2** quite high performance for the C_2H_6/C_2H_4 separation. Moreover, compared with MOF [Cu(Qc)$_2$], **Ni-MOF-2** possesses larger surface area and pore volume, therefore it exhibits much higher C_2H_4 productivity of $12 \, L \, kg^{-1}$ over $4.3 \, L \, kg^{-1}$ for [Cu(Qc)$_2$] although the latter one has higher separation selectivity (the overall productivity is correlated to gas separation selectivity, uptake and pore volume). It is

[*] Dr. Y. Ye, Dr. L. Gong, Dr. J. Phipps, Prof. S. Ma
Department of Chemistry, University of North Texas
1508 W Mulberry St., Denton, TX 76201 (USA)
E-mail: shengqian.ma@unt.edu

Dr. Y. Ye, Dr. L. Gong, Prof. B. Chen
College of Chemistry and Materials Science, Fujian Normal University
Fuzhou 350007 (China)
E-mail: banglin.chen@fjnu.edu.cn

Y. Xie, Dr. Y. Shi
Department of Chemistry, University of Texas at San Antonio
One UTSA Circle, San Antonio, TX 78249 (USA)

Prof. A. M. Al-Enizi, Prof. A. Nafady
Department of Chemistry, College of Science, King Saud University
Riyadh, 11451 (Saudi Arabia)

worth further noting that separation potential (Δq) of **Ni-MOF 2** from equimolar C_2H_6/C_2H_4 is up to 1.7 mmol g^{-1}, which is comparable to those of benchmark materials, such as CPM-733 (1.88 mmol g^{-1})[10] and Fe$_2$(O$_2$)(dobdc) (1.74 mmol g^{-1}),[11] and outperforms most reported C_2H_6-selective adsorbents under similar conditions.

Results and Discussion

The pair of isoreticular MOFs (**Ni-MOF 1** and **Ni-MOF 2**) were synthesized according to previously reported procedures with some modifications.[12] The PXRD patterns of the as-synthesized sample match well with the calculated ones, indicating that this pair of MOFs have been successfully synthesized with high purity (Figure S6). In **Ni-MOF 1**, each Ni^{II} ion is six-coordinated by four triazole groups (with four N atoms) and two Cl$^-$ ions, forming an octahedral geometry, which is expanded to adjacent Ni^{II} atoms by bridging Cl$^-$ ions and triazole (tz) groups affording a one-dimensional chain of [NiCl(tz)$_2$]$_n^{n+}$ (Figure 1a). This 1D chain is further connected to four neighboring chains by neutral btz ligands to build a 3D cationic open framework housing a 1D rhomboidal channel, and providing counter chloride ions to balance the frameworks' charge. In contrast, the crystallographically independent Ni^{2+} ion in **Ni-MOF 2** is coordinated by four pyrazolyl groups with four N atoms, generating a typical square-planar geometry. Notably, the Ni^{2+} ion in **Ni-MOF 2** is only extended through pyrazolyl (pz) groups affording one-dimensional [Ni(Pz)$_2$]$_n$ chain, which is further linked by bdp linkers to construct a 3D neutral open framework with a similar 1D rhombic channel (Figure 1b). Compared with **Ni-MOF 2**, the counter anions (Cl$^-$) within the 1D channel of **Ni-MOF 1** not only block part of the pore
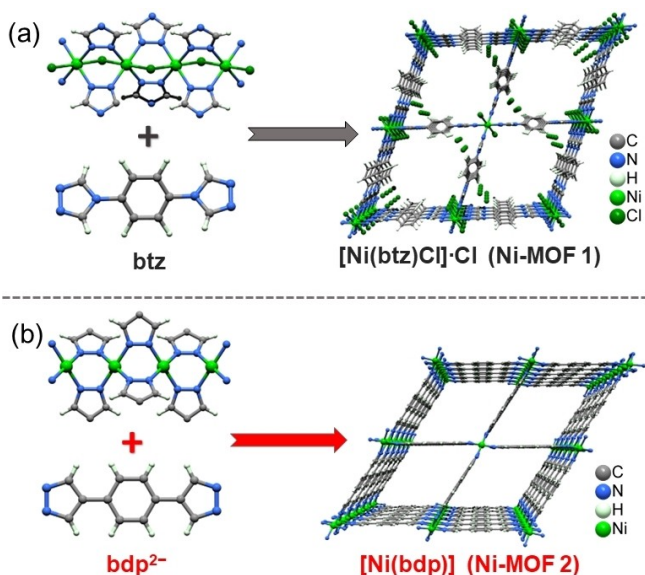
spaces, but also may affect the effective roles of the three aromatic rings for their interactions with guest molecules (Figure S2).

The permanent porosities of these two MOFs were verified by nitrogen sorption experiments at 77 K. As shown in Figures S7 and S8, the N$_2$ sorption isotherms of **Ni-MOF 1** and **Ni-MOF 2** both display the fully reversible type I adsorption behaviors, indicating their typical microporous features. The Brunauer–Emmett–Teller (BET) surface areas were calculated to be 1262 and 1501 m^2 g^{-1} for **Ni-MOF 1** and **Ni-MOF 2** respectively from N$_2$ adsorption isotherms, which match well with the previously reported values.[12a, 13] The pore size distributions of these two MOFs were also deduced from the 77 K N$_2$ isotherms using the non-local density functional theory (NLDFT) model, with the calculated pore sizes of 6.8 Å for **Ni-MOF 1** and 8.0 Å for **Ni-MOF 2** (Figure S9).

The low-pressure C_2H_6 and C_2H_4 single-component adsorption data were then collected under ambient conditions. As depicted in Figure 2a, **Ni-MOF 1** yields an almost identical sorption behavior for C_2H_6 and C_2H_4, with the uptake capacity of 113 cm^3 g^{-1} and 116 cm^3 g^{-1} respectively at 298 K and 1 bar. In contrast, **Ni-MOF 2** showed an obviously clear preferential adsorption of ethane over ethylene, in which the C_2H_6 uptake value (133 cm^3 g^{-1}) is notably higher than that of C_2H_4 (105 cm^3 g^{-1}) at ambient conditions. This finding is consistent with the calculated isosteric heat of adsorption (Q_{st}) of the material. As shown in Figure S17, the Q_{st} value of C_2H_6 (23.6 kJ mol^{-1}) in **Ni-MOF 2** at near-zero coverage is higher than that of C_2H_4 (21.4 kJ mol^{-1}), indicating this MOF has a stronger affinity for C_2H_6 over C_2H_4. In comparison, the Q_{st} of **Ni-MOF 1** for C_2H_6 and C_2H_4 is 27.2 and 28.5 kJ mol^{-1}, respectively. This indicates that the adsorbent-adsorbate interactions in **Ni-MOF 1** are notably higher than that in **Ni-MOF 2** at low gas coverage area, which is in good agreement with the results of the adsorption isotherms (Figure S14).

The C_2H_6 uptake capacity of **Ni-MOF 2** at 1 bar (5.94 mmol g^{-1}) is comparable to those of CPM-733 (7.1 mmol g^{-1}),[10] Ni(TMBDC)(DABCO)$_{0.5}$ (5.2 mmol g^{-1}),[14] and PCN-250 (5.2 mmol g^{-1}),[15] and notably higher than those of the representative ethane-selective adsorbents, such as ZJU-HOF-1 (4.87 mmol g^{-1}),[16] NKCOF-21 (4.4 mmol g^{-1}),[17] Fe$_2$(O$_2$)(dobdc) (3.32 mmol g^{-1}),[11] Cu(Qc)$_2$ (1.85 mmol g^{-1}),[9d] and MAF-49 (1.73 mmol g^{-1}),[18] under similar conditions. Furthermore, at a partial pressure of 0.5 bar for equimolar a C_2H_6/C_2H_4 mixture, the C_2H_6 uptake value (4.7 mmol g^{-1}) of **Ni-MOF 2** continues to surpass SNNU-40 (3.34 mmol g^{-1}),[19] PCN-250 (4.3 mmol g^{-1}),[15] ZJU-120 (4.29 mmol g^{-1}),[20] and other top performing C_2H_6/C_2H_4 separation materials (Figure 2c).[9a–d, 11, 21] It's worth noting that the difference of uptake capacity (ΔQ) between C_2H_6 and C_2H_4 at 0.5 bar in **Ni-MOF 2** is up to 1.74 mmol g^{-1}, defined as $\Delta Q = Q_{C_2H_6} - Q_{C_2H_4}$, which is the highest value among the reported C_2H_6-selective porous materials.

Upon observing the exceptional C_2H_6-selective adsorption behavior and higher ethane-binding affinity, the widely studied ideal adsorbed solution theory (IAST) was em-
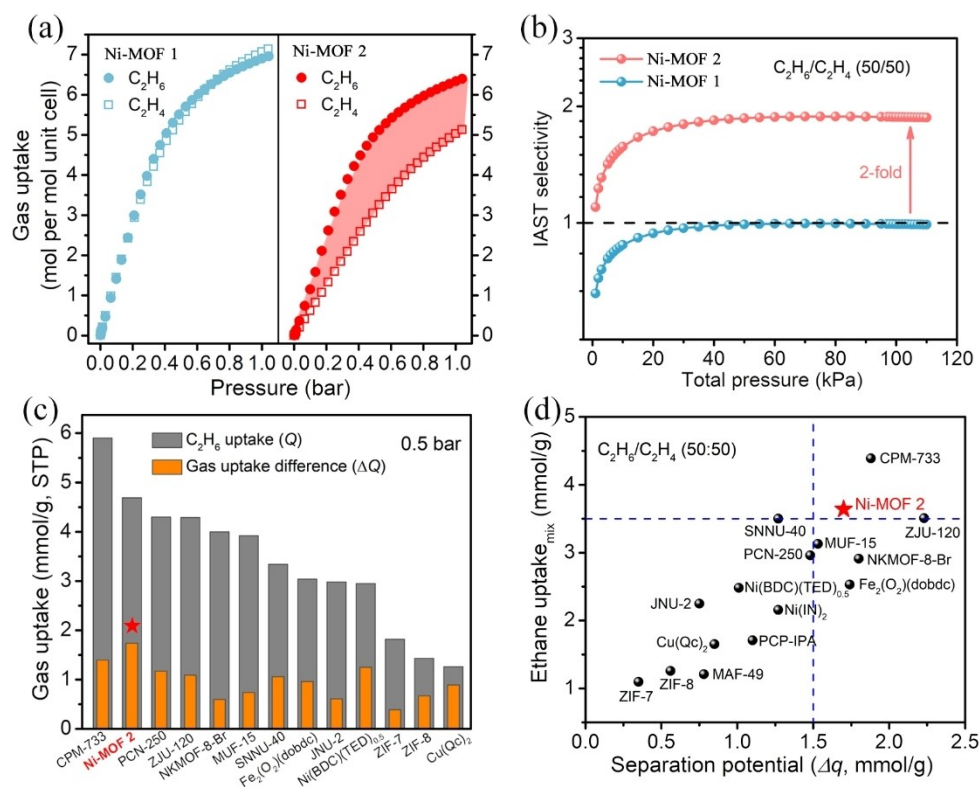
Figure 1. Schematic diagram depicting the starting materials and the three-dimensional open framework of synthesized a) **Ni-MOF 1**, and b) **Ni-MOF 2**.

Figure 2. a) C_2H_4 and C_2H_6 single-component adsorption isotherms of **Ni-MOF 1** and **Ni-MOF 2** at 298 K. b) The IAST selectivity of **Ni-MOF 1** and **Ni-MOF 2** for equimolar C_2H_6/C_2H_4. c) Comparison of the C_2H_6 uptake and C_2H_6-C_2H_4 uptake differences of **Ni-MOF 2** with other representative porous materials from static adsorption isotherms at 0.5 bar and room temperature. d) Comparison of the C_2H_6 uptake and separation potential Δq from equimolar C_2H_6/C_2H_4 mixtures of **Ni-MOF 2** with other representative C_2H_6-selective porous adsorbents at ambient conditions.

ployed to calculate the C_2H_6/C_2H_4 separation selectivity.[22] Consistent with our other results, the IAST selectivity of **Ni-MOF 2** for binary C_2H_6/C_2H_4 (50/50) mixtures is up to 1.9 at 298 K and 100 kPa, which is about 2-fold higher than that of **Ni-MOF 1** (1.0, Figure 2b) and comparable to some of the top-performing C_2H_6-selective materials, e.g. MUF-15 (1.96),[21a] CPM-733 (1.75),[10] and HOF-76 (2.0).[23] Although high C_2H_6/C_2H_4 separation selectivity has been observed in some porous materials, their inferior C_2H_6 adsorption capacity also restricts their final separation performance. To overcome this dilemma, we utilized a combined metric termed as separation potential $(\Delta q = q_{C_2H_6}\frac{y_{C_2H_4}}{1-y_{C_2H_4}} - q_{C_2H_4})$ to evaluate the C_2H_6/C_2H_4 separation performance, which was firstly defined by Krishna (See Supporting Information for details).[24] As expected, **Ni-MOF 2** shows a relatively high separation potential $(\Delta q = 1.7\ \text{mmol}\,\text{g}^{-1})$ for a C_2H_6/C_2H_4 (50/50) mixture, which is comparable to benchmark materials CPM-733 $(1.88\ \text{mmol}\,\text{g}^{-1})$[10] and $Fe_2(O_2)(dobdc)$ $(1.74\ \text{mmol}\,\text{g}^{-1})$,[11] and outperforms most reported C_2H_6-selective adsorbents (Figure 2d).[25]

To gain deeper insights into the origin of the dramatically different C_2H_6/C_2H_4 separation performance of this pair of isoreticular MOFs, theoretical calculations were performed based on first-principles dispersion-corrected density functional theory (DFT-D). Optimal adsorption configurations of C_2H_6 and C_2H_4 were identified and are schematically depicted in Figure 3. From these results, it can
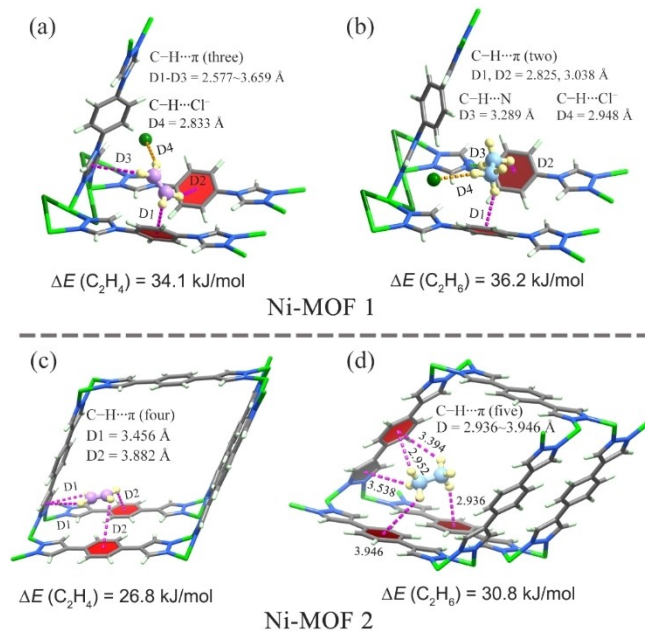

Figure 3. Comparison of the primary binding sites of C_2H_4 (left) and C_2H_6 (right) in a), b) **Ni-MOF 1** and c), d) **Ni-MOF 2** observed by Density-Functional Theory (DFT) optimizations.

be observed that both C_2H_6 and C_2H_4 molecules are located at the cavities of the pores in **Ni-MOF 1**, but with different molecular orientations. In this position, the three hydrogen atoms of C_2H_4 can interact with three adjacent aromatic rings (two phenyl and a pyrazolyl) to form multiple C–H⋯π van der Waals (vdW) interactions (2.577 to 3.659 Å), and the fourth H atoms is close to the counter Cl^- ion (C–H⋯Cl, D = 2.833 Å). Similarly, only four hydrogen atoms in the C_2H_6 molecule could generate C–H⋯π, C–H⋯N, and C–H⋯Cl interactions with aromatic rings and counter-anions, with the close distances ranging from 2.825 to 3.289 Å. Due to the almost identical host–guest multiple interactions, **Ni-MOF 1** displays similar binding energies for C_2H_4 (34.1 kJ mol^{-1}) and C_2H_6 (36.2 kJ mol^{-1}). On the other hand, in **Ni-MOF 2**, the C_2H_6 molecule is adsorbed at the pore corners, where the five hydrogen atoms of C_2H_6 can interact with four adjacent aromatic rings (three phenyl and a pyrazolyl) to form multiple C–H⋯π van der Waals (vdW) interactions, with the close distances ranging from 2.936 to 3.946 Å. In contrast, the planar C_2H_4 molecule is perpendicular to the MOF channel, and shows contacts only with three adjacent aromatic rings (two phenyl and a pyrazolyl) with the longer C–H⋯π distances of 3.456–3.882 Å. As a result, the higher polarizability, more and stronger C–H⋯π interactions result in a stronger binding affinity of **Ni-MOF 2** for C_2H_6 over C_2H_4, as indicated by the higher calculated binding energies of C_2H_6 (30.8 kJ mol^{-1}) than C_2H_4 (26.8 kJ mol^{-1}). These theoretical calculation results are fully consistent with our experimental findings discussed earlier.

To understand the effectiveness in separation performance, we examined the materials under real-world conditions. To accomplish this, equimolar C_2H_6/C_2H_4 mixtures were flowed through a packed column filled with activated **Ni-MOF 2** sample at a flow rate of 2 mL min^{-1}. As predicted, the C_2H_6/C_2H_4 gas mixture can be efficiently separated by using activated **Ni-MOF 2**, in which C_2H_4 was first eluted at 49 min, and quickly achieved a polymer grade purity (over 99.95 %) without a detectable C_2H_6 signal (Figure 4a). After a period ($\approx$10 min), the adsorbent was saturated in the dynamic gas mixture flow, thus allowing the preferential adsorption component C_2H_6 through after reaching its breakthrough point at 59 min. According to the C_2H_6/C_2H_4 breakthrough curve, **Ni-MOF 2** can directly produce a productivity of 12 L kg^{-1} high-purity C_2H_4 under a given

cycle, which is comparable to MUF-15 (14 L kg^{-1})[21a] and PCN-250 (10 L kg^{-1}),[15] and exceeds that of MAF-49 (6.3 L kg^{-1}),[18] Cu(Qc)$_2$ (4.3 L kg^{-1}),[9d] and HOF-76 (7.2 L kg^{-1}).[23] Meanwhile, the dynamic ethane capture amounts of **Ni-MOF 2** were calculated to be 2.0 mol kg^{-1}. It needs to be particularly mentioned that although the strategy developed here is almost the same as that we realized before for Cu(Qc)$_2$ (4.3 L kg^{-1}),[9d] such a strategy has been rarely realized. Furthermore, the current **Ni-MOF 2** has much higher C_2H_4 productivity of 12 L kg^{-1} than 4.3 L kg^{-1} for Cu(Qc)$_2$. While good adsorption is preferable, facile regeneration and good repeatability are essential for the practical application of porous adsorbents. To examine these factors, we performed multicycle mixed-gas break-through experiment under the same conditions. As depicted in Figure 4b, the results indicate that breakthrough performance of **Ni-MOF 2** remains virtually unchanged for five consecutive cycles, demonstrating its good reproducibility for this separation. Notably, this MOF only needs to be regenerated by a simple inert purge under ambient conditions. Such a simple process has significant implications for energy-efficient separations in the future. Furthermore, the stability of **Ni-MOF 2** toward air/water humidity, acid-base environment and after cycling experiments was further proved by gas adsorption isotherms and/or PXRD patterns (Figures S25–S28).

Conclusion

In summary, we report a microporous MOF (**Ni-MOF 2**) with unique aromatic pore surfaces for high performance C_2H_6/C_2H_4 separation. The naked aromatic pore surfaces within **Ni-MOF 2** can form more and stronger C–H⋯π interactions with C_2H_6 molecules over C_2H_4 ones, which is well supported by gas sorption isotherms, breakthrough experiments and molecular modeling studies. This study not only clearly establishes the rich aromatic pore surfaces for their stronger C–H⋯π interactions with C_2H_6 molecules as a general approach for fulfilling high performance C_2H_6/C_2H_4 separation, but also significantly enhances the polymer-grade C_2H_4 productivity of 12 L kg^{-1} from the highest reported 4.3 L kg^{-1} in Cu(Qc)$_2$. Given the fact that no systematic approaches have been established yet for developing high performance porous materials for C_2H_6/C_2H_4 separation, this work opens the door of realizing even higher performance porous materials more rationally for this industrially very important gas separation in the future.
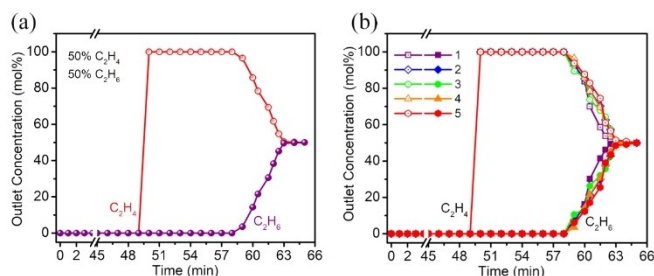

Figure 4. a), b) Single and multicycle dynamic breakthrough curves of equimolar C_2H_6/C_2H_4 gas mixtures through a separation column filling with **Ni-MOF 2** sample at 298 K and 1 bar.

Angewandte
International Edition Chemie

Conflict of Interest

The authors declare no conflict of interest.

Data Availability Statement

The data that support the findings of this study are available from the corresponding author upon reasonable request.

Keywords: Aromatic Pore Surfaces · C_2H_6/C_2H_4 Separation · Gas Adsorption · Metal–Organic Framework

[1] R. B. Eldridge, *Ind. Eng. Chem. Res.* **1993**, *32*, 2208–2212.

[2] a) S. Chu, Y. Cui, N. Liu, *Nat. Mater.* **2017**, *16*, 16–22; b) M. H. Mohamed, Y. Yang, L. Li, S. Zhang, J. P. Ruffley, A. G. Jarvi, S. Saxena, G. Veser, J. K. Johnson, N. L. Rosi, *J. Am. Chem. Soc.* **2019**, *141*, 13003–13007.

[3] a) Y. Wang, S. B. Peh, D. Zhao, *Small* **2019**, *15*, 1900058; b) H. Wang, D. Luo, E. Velasco, L. Yu, J. Li, *J. Mater. Chem. A* **2021**, *9*, 20874–20896.

[4] a) R. B. Lin, L. Li, H. L. Zhou, H. Wu, C. He, S. Li, R. Krishna, J. Li, W. Zhou, B. Chen, *Nat. Mater.* **2018**, *17*, 1128–1133; b) Z. Bao, J. Wang, Z. Zhang, H. Xing, Q. Yang, Y. Yang, H. Wu, R. Krishna, W. Zhou, B. Chen, Q. Ren, *Angew. Chem. Int. Ed.* **2018**, *57*, 16020–16025; c) C. Gu, N. Hosono, J. J. Zheng, Y. Sato, S. Kusaka, S. Sakaki, S. Kitagawa, *Science* **2019**, *363*, 387–391; d) Y. Yang, L. Li, R. B. Lin, Y. Ye, Z. Yao, L. Yang, F. Xiang, S. Chen, Z. Zhang, S. Xiang, B. Chen, *Nat. Chem.* **2021**, *13*, 933–939.

[5] D. F. Lv, P. J. Zhou, J. H. Xu, S. Tu, F. Xu, J. Yan, H. X. Xi, W. B. Yuan, Q. Fu, X. Chen, Q. B. Xia, *Chem. Eng. J.* **2022**, *431*, 133208.

[6] a) H. Furukawa, K. E. Cordova, M. O'Keeffe, O. M. Yaghi, *Science* **2013**, *341*, 1230444; b) X. Zhao, Y. Wang, D. S. Li, X. Bu, P. Feng, *Adv. Mater.* **2018**, *30*, 1705189; c) R. B. Lin, Z. Zhang, B. Chen, *Acc. Chem. Res.* **2021**, *54*, 3362–3376; d) X. Cui, K. Chen, H. Xing, Q. Yang, R. Krishna, Z. Bao, H. Wu, W. Zhou, X. Dong, Y. Han, B. Li, Q. Ren, M. J. Zaworotko, B. Chen, *Science* **2016**, *353*, 141–144; e) A. Cadiau, K. Adil, P. M. Bhatt, Y. Belmabkhout, M. Eddaoudi, *Science* **2016**, *353*, 137–140; f) Y. Ye, Z. Ma, R.-B. Lin, R. Krishna, W. Zhou, Q. Lin, Z. Zhang, S. Xiang, B. Chen, *J. Am. Chem. Soc.* **2019**, *141*, 4130–4136; g) J. B. Lin, T. T. T. Nguyen, R. Vaidhyanathan, J. Burner, J. M. Taylor, H. Durekova, F. Akhtar, R. K. Mah, O. Ghaffari-Nik, S. Marx, N. Fylstra, S. S. Iremonger, K. W. Dawson, P. Sarkar, P. Hovington, A. Rajendran, T. K. Woo, G. K. H. Shimizu, *Science* **2021**, *374*, 1464–1469; h) Y. Ye, S. Xian, H. Cui, K. Tan, L. Gong, B. Liang, T. Pham, H. Pandey, R. Krishna, P. C. Lan, K. A. Forrest, B. Space, T. Thonhauser, J. Li, S. Ma, *J. Am. Chem. Soc.* **2022**, *144*, 1681–1689.

[7] a) E. D. Bloch, W. L. Queen, R. Krishna, J. M. Zadrozny, C. M. Brown, J. R. Long, *Science* **2012**, *335*, 1606–1610; b) B. Li, Y. Zhang, R. Krishna, K. Yao, Y. Han, Z. Wu, D. Ma, Z. Shi, T. Pham, B. Space, J. Liu, P. K. Thallapally, J. Liu, M. Chrzanowski, S. Ma, *J. Am. Chem. Soc.* **2014**, *136*, 8654–8660; c) L. Zhang, L. Li, E. Hu, L. Yang, K. Shao, L. Yao, K. Jiang, Y. Cui, Y. Yang, B. Li, B. Chen, G. Qian, *Adv. Sci.* **2020**, *7*, 1901918.

[8] J. R. Li, R. J. Kuppler, H. C. Zhou, *Chem. Soc. Rev.* **2009**, *38*, 1477–1504.

[9] a) C. Gücüyener, J. van den Bergh, J. Gascon, F. Kapteijn, *J. Am. Chem. Soc.* **2010**, *132*, 17704–17706; b) U. Böhme, B. Barth, C. Paula, A. Kuhnt, W. Schwieger, A. Mundstock, J. Caro, M. Hartmann, *Langmuir* **2013**, *29*, 8592–8600; c) W. Liang, F. Xu, X. Zhou, J. Xiao, Q. Xia, Y. Li, Z. Li, *Chem. Eng. Sci.* **2016**, *148*, 275–281; d) R. B. Lin, H. Wu, L. Li, X. L. Tang, Z. Li, J. Gao, H. Cui, W. Zhou, B. Chen, *J. Am. Chem. Soc.* **2018**, *140*, 12940–12946; e) M. Kang, S. Yoon, S. Ga, D. W. Kang, S. Han, J. H. Choe, H. Kim, D. W. Kim, Y. G. Chung, C. S. Hong, *Adv. Sci.* **2021**, *8*, 2004940.

[10] H. Yang, Y. Wang, R. Krishna, X. Jia, Y. Wang, A. N. Hong, C. Dang, H. E. Castillo, X. Bu, P. Feng, *J. Am. Chem. Soc.* **2020**, *142*, 2222–2227.

[11] L. Li, R. B. Lin, R. Krishna, H. Li, S. Xiang, H. Wu, J. Li, W. Zhou, B. Chen, *Science* **2018**, *362*, 443–446.

[12] a) S. Galli, N. Masciocchi, V. Colombo, A. Maspero, G. Palmisano, F. J. Lopez-Garzon, M. Domingo-Garcia, I. Fernandez-Morales, E. Barea, J. A. R. Navarro, *Chem. Mater.* **2010**, *22*, 1664–1672; b) L. Wang, Y. Ye, Z. Li, Q. Lin, J. Ouyang, L. Liu, Z. Zhang, S. Xiang, *Cryst. Growth Des.* **2017**, *17*, 2081–2089.

[13] G. Huang, L. Yang, Q. Yin, Z. B. Fang, X. J. Hu, A. A. Zhang, J. Jiang, T. F. Liu, R. Cao, *Angew. Chem. Int. Ed.* **2020**, *59*, 4385–4390.

[14] X. Wang, Z. Niu, A. M. Al-Enizi, A. Nafady, Y. F. Wu, B. Aguila, G. Verma, L. Wojtas, Y. S. Chen, Z. Li, S. Q. Ma, *J. Mater. Chem. A* **2019**, *7*, 13585–13590.

[15] Y. W. Chen, Z. W. Qiao, H. X. Wu, D. F. Lv, R. F. Shi, Q. B. Xia, J. Zhou, Z. Li, *Chem. Eng. Sci.* **2018**, *175*, 110–117.

[16] X. Zhang, J. X. Wang, L. Li, J. Pei, R. Krishna, H. Wu, W. Zhou, G. Qian, B. Chen, B. Li, *Angew. Chem. Int. Ed.* **2021**, *60*, 10304–10310.

[17] F. Jin, E. Lin, T. Wang, S. Geng, T. Wang, W. Liu, F. Xiong, Z. Wang, Y. Chen, P. Cheng, Z. Zhang, *J. Am. Chem. Soc.* **2022**, *144*, 5643–5652.

[18] P. Q. Liao, W. X. Zhang, J. P. Zhang, X. M. Chen, *Nat. Commun.* **2015**, *6*, 8697.

[19] Y. P. Li, Y. N. Zhao, S. N. Li, D. Q. Yuan, Y. C. Jiang, X. Bu, M. C. Hu, Q. G. Zhai, *Adv. Sci.* **2021**, *8*, 2003141.

[20] J. Y. Pei, J. X. Wang, K. Shao, Y. Yang, Y. J. Cui, H. Wu, W. Zhou, B. Li, G. D. Qian, *J. Mater. Chem. A* **2020**, *8*, 3613–3620.

[21] a) O. T. Qazvini, R. Babarao, Z. L. Shi, Y. B. Zhang, S. G. Telfer, *J. Am. Chem. Soc.* **2019**, *141*, 5014–5020; b) H. Zeng, X. J. Xie, M. Xie, Y. L. Huang, D. Luo, T. Wang, Y. Zhao, W. Lu, D. Li, *J. Am. Chem. Soc.* **2019**, *141*, 20390–20396; c) S. Geng, E. Lin, X. Li, W. Liu, T. Wang, Z. Wang, D. Sensharma, S. Darwish, Y. H. Andaloussi, T. Pham, P. Cheng, M. J. Zaworotko, Y. Chen, Z. Zhang, *J. Am. Chem. Soc.* **2021**, *143*, 8654–8660.

[22] A. L. Myers, J. M. Prausnitz, *AIChE J.* **1965**, *11*, 121–127.

[23] X. Zhang, L. Li, J. X. Wang, H. M. Wen, R. Krishna, H. Wu, W. Zhou, Z. N. Chen, B. Li, G. Qian, B. Chen, *J. Am. Chem. Soc.* **2020**, *142*, 633–640.

[24] R. Krishna, *ACS Omega* **2020**, *5*, 16987–17004.

[25] a) H. G. Hao, Y. F. Zhao, D. M. Chen, J. M. Yu, K. Tan, S. Ma, Y. Chabal, Z. M. Zhang, J. M. Dou, Z. H. Xiao, G. Day, H. C. Zhou, T. B. Lu, *Angew. Chem. Int. Ed.* **2018**, *57*, 16067–16071; b) A. A. Lysova, D. G. Samsonenko, K. A. Kovalenko, A. S. Nizovtsev, D. N. Dybtsev, V. P. Fedin, *Angew. Chem. Int. Ed.* **2020**, *59*, 20561–20567; c) K. Su, W. Wang, S. Du, C. Ji, D. Yuan, *Nat. Commun.* **2021**, *12*, 3703; d) C. X. Chen, Z. W. Wei, T. Pham, P. C. Lan, L. Zhang, K. A. Forrest, S. Chen, A. M. Al-Enizi, A. Nafady, C. Y. Su, S. Ma, *Angew. Chem. Int. Ed.* **2021**, *60*, 9680–9685; e) Y. Wang, C. Hao, W. Fan, M. Fu, X. Wang, Z. Wang, L. Zhu, Y. Li, X. Lu, F. Dai, Z. Kang, R. Wang, W. Guo, S. Hu, D. Sun, *Angew. Chem. Int. Ed.* **2021**, *60*, 11350–11358; f) L. Guo, M. Savage, J. H. Carter, X. Han, I. da Silva, P. Manuel, S. Rudic, C. C. Tang, S. Yang, M. Schroder, *Chem. Mater.* **2022**, *34*, 5698–5705; g) Z. Di, C. Liu, J. Pang, S. Zou, Z. Ji, F. Hu, C. Chen, D. Yuan, M. Hong, M.

Wu, *Angew. Chem. Int. Ed.* **2022**, *61*, e202210343; h) P. Zhang, L. Yang, X. Liu, J. Wang, X. Suo, L. Chen, X. Cui, H. Xing, *Nat. Commun.* **2022**, *13*, 4928; i) L. Yang, L. Yan, W. Niu, Y. Feng, Q. Fu, S. Zhang, Y. Zhang, L. Li, X. Gu, P. Dai, D. Liu, Q. Zheng, X. Zhao, *Angew. Chem. Int. Ed.* **2022**, *61*, e202204046; j) G. D. Wang, R. Krishna, Y. Z. Li, W. J. Shi, L. Hou, Y. Y. Wang, Z. Zhu, *Angew. Chem. Int. Ed.* **2022**, *61*, e202213015; k) S. S. Jiang, J. Q. Li, M. Feng, R. D. Chen, L. D. Guo, Q. Q. Xu, L. H. Chen, F. X. Shen, Z. G. Zhang, Y. W. Yang, Q. L. Ren, Q. W. Yang, Z. B. Bao, *J. Mater. Chem. A* **2022**, *10*, 24127–24136.